Advanced Steel Construction – Vol. 22 No. 3 (2026) 331–343
DOI:10.18057/IJASC.2026.22.3.9

RESEARCH ON THE EXTERNAL RESTRAINED UNITS STIFFNESS OF SEGMENTED ASSEMBLED BUCKLING-RESTRAINED BRACES

Shuai Xu [1, 2], Cheng-Xin Guo [1, *], Yan Li [1, 2], Xiu-Li Wang [1, 2], Mei-Qiu Zhan [1, 2] and Yuan-Hong Hu [1]

[1] *School of Civil Engineering, Jilin Jianzhu University, Changchun 130118, China*

[2] *Key Laboratory of Architectural Cold Climate Energy Management, Ministry of Education, Jilin Jianzhu University, Changchun 130118, China*

* *(Corresponding author: E-mail: guochengxin@student.jlju.edu.cn)*

A B S T R A C T

The peripheral units of the novel segmented assembled buckling-restrained braces (SABRBs) are assembled by connecting the upper and lower restrained cover plates to the lateral C-shaped steel restraint units using multiple sets of bolts. Owing to the discontinuity of the lateral restraint units, calculating the restraint stiffness becomes relatively complex. In comparison with integrally restrained BRBs, SABRBs necessitate additional consideration of the effects arising from bolt installation. Given the non-uniform lateral forces transferred from the inner core plate to the C-shaped steel restrained units, the SABRBs are assumed to rotate about their width axis. The reduction in stiffness of the peripheral restrained units is primarily attributed to torsional deformation of the plates adjacent to the bolts. In this study, a mechanical model is established that incorporates both the flexibility of bolted connections and the effective area of the restrained plates. By analyzing the deformation mechanism of the peripheral restrained units in the segmented assembled SABRBs, the corresponding force transfer process is examined. Through theoretical derivation and numerical analysis, a formula for the stiffness reduction coefficient μ0y is derived. Strategies such as optimizing segment layout and adding stiffeners to laterally restrained units are proposed to control this coefficient. Finally, a calculation method for the stiffness of peripheral restrained units is presented. The proposed formula is validated using parametric finite element analyses and experimental data.

A R T I C L E   H I S T O R Y

Received: 10 September 2025
Revised: 17 January 2026
Accepted: 22 January 2026

K E Y W O R D S

Deformation mechanism;
Assembled buckling-restrained brace;
Restrained Stiffness

1. Introduction

BRBs are highly efficient energy-dissipating and seismic-mitigation units [1-5]. They mainly consist of an axial force-resisting core plate, an outer restrained unit that prevents the core from buckling, and an intermediate unbonded material layer. In recent years, with the rapid development of high-rise and super high-rise buildings both domestically and internationally, assembled BRBs have been increasingly applied in practical engineering. This is due to the advantages of BRBs, such as lightweight construction, ease of installation, replaceable cores after an earthquake, cost-effectiveness and environmental sustainability. Consequently, the types and design theories of BRBs have become more sophisticated [6-13]. Traditional BRBs typically use integrally fabricated restrained units. While this design ensures adequate restrained stiffness, it involves complex manufacturing processes. Furthermore, post-earthquake repairs necessitate replacing the entire BRB assembly, resulting in higher costs and greater operational complexity. Large-tonnage or extra-long BRBs are required for engineering projects, but the use of integral BRBs presents substantial transportation and installation challenges. To address these issues, Zhang Ailin [14] proposed a two-stage assembled BRB, which offers advantages in transportation and installation. Their research confirmed that steel frame-BRB systems incorporating two-stage assembled BRBs exhibit excellent seismic performance. Similarly, Li Guochang [15] developed a novel assembled BRB featuring full-angle steel-restrained units and an aluminum alloy core, demonstrating that it delivers favorable energy dissipation and fatigue resistance while retaining economic and environmental benefits. This study focuses on a segmented assembled BRB [16], as illustrated in Fig. 1. Its external Restrained Units comprise multiple units connected by bolts. Compared with integral BRBs, this configuration significantly simplifies fabrication, transportation, and installation. Additionally, the assembled buckling-restrained brace (BRB) is composed of restrained cover plates, restrained side plates, and a core plate, which are rigidly connected by bolts. These components collectively form an enclosed cavity slightly larger than the core plate—a design intended to allow the core plate ample deformation space under loading. This ensures the core plate can fully harness its energy-dissipating capability, thereby enhancing the structural seismic performance. A notable advantage of the assembled BRB emerges during post-earthquake building repair: only the core plate needs individual replacement, while the external restrained units can be reused intact [17].

The force transmission mechanism of this new segmented assembled BRB differs markedly from that of the conventional integral BRB. The external Restrained Units are bolt-connected and exhibit longitudinal discontinuity, leading to a non-uniform longitudinal stiffness distribution. Accurate assessment of the stiffness of the external Restrained Units is therefore crucial for the structural design of SABRBs.

A new mechanical model is developed that explicitly represents the deformation mechanism of bolt-connected restraining units. The model introduces the concept of effective plate width to quantify the participatory area of cover and side plates in load transfer, and formulates the stiffness reduction via newly derived coefficients. These coefficient captures the combined effects of bolt spacing, bolt cross-sectional position, and the torsional deformation of plates adjacent to bolts—factors previously unquantified in integral BRB design. Key parameters in the theoretical model, namely the effective width coefficients and the stiffness reduction coefficient are determined through extensive parametric finite element analysis. Empirical relationships are established via curve fitting, expressing these coefficients as functions of bolt spacing and the geometric parameters. These fitted equations enable practical design application without requiring complex numerical simulations for each case. The proposed methodology is intended for the design and stiffness evaluation of SABRBs with bolted C-shaped steel restraining units and straight core plates. It applies to braces under elastic behavior of restraining units and does not account for material yielding or bolt preload effects. The method is intended for assembled segmented BRBs with bolted connections.

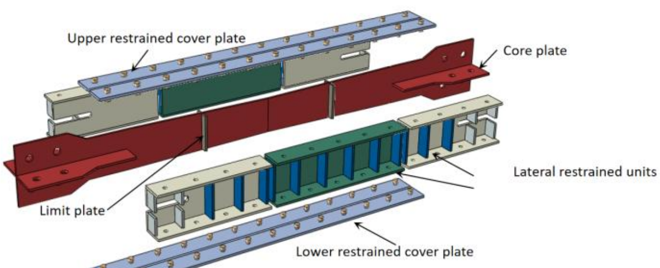

Fig. 1 Disassembly schematic of SABRB

Fig. 2 shows a schematic cross-sectional view of the segmented assembled buckling-restrained brace (BRB), with several key geometric parameters clearly labeled.

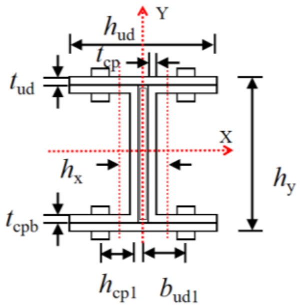

Fig. 2 Sectional schematic of SABRB

In Fig. 2, the width and thickness of the upper (and lower) restrained cover plates are denoted as h_{ud} and t_{ud}, respectively. The height and thickness of the left (and right) lateral restrained units are denoted as h_{cp} and t_{cp}, while the flange width and flange thickness of the left (and right) restrained units are b_{cp} and t_{cpb}, respectively. The distance from the bolt center to the neutral axis of the flange is defined as h_{cp1}, and the distance from the bolt center to the mid-plane of the upper (and lower) restrained cover plates is b_{ud1}. The distance between the neutral axes of the left and right restrained units is denoted as h_x, and the overall height of the external Restrained Units is represented by h_y.

The stiffness performance of the external Restrained Units is primarily reflected in their deformation under the lateral compressive force exerted by the core plate. In this study, the factors influencing the restrained stiffness are investigated by analyzing the deformation behavior of the restrained units.

2. Analysis of factors influencing the stiffness of the external restrained units

2.1. Simplified model

Under axial compression, the SABRB exhibits two-point contact between the core plate and the external Restrained Units at its ends. The lateral compressive force acting at the mid-span can be approximated as a sinusoidally distributed load [18–19]. Thus, the external Restrained Units can be modeled as a simply supported beam subjected to concentrated loads at both ends and a sinusoidally distributed load at the mid-span.

Based on the simplified analysis methods for assembled buckling-restrained braces (BRBs) presented in References 20 and 23, this paper idealizes and simplifies the external restraint units into a three-layer truss system by considering their composition and force transmission characteristics. A half-span of the original system is extracted as the equivalent simplified model: one end, corresponding to the mid-span of the actual structure, is defined as a fixed end; the other end, representing the structural end, is defined as a free end. The equivalent simplified model is illustrated in Fig. 3.

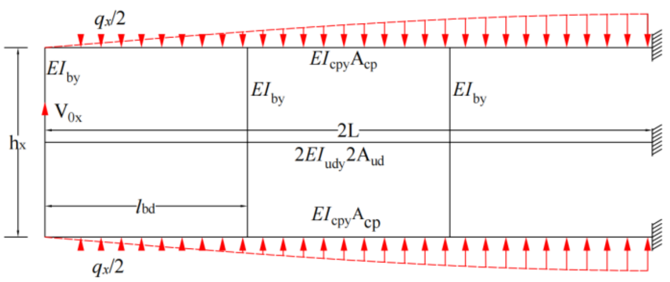

Fig. 3 Equivalent simplified model

The upper and lower chords of the equivalent simplified model represent the left and right lateral restrained units, each with a bending stiffness of EI_{cpy} and a cross-sectional area of A_{cp}. The middle chord represents the upper and lower restrained cover plates, with a combined bending stiffness of $2EI_{udy}$ and a total cross-sectional area of $2A_{ud}$. Specific units of the external Restrained Units, together with the bolts, are modeled as web members in the truss system. The spacing between web members corresponds to the distance between adjacent bolts, denoted as l_{bd}, and their bending stiffness—denoted as EI_{by}—is to be determined.

2.2. Influencing factors

For this type of SABRB, if all units are tightly connected, they can theoretically be assumed to function as a fully composite system. However, due to imperfect connectivity between units, the overall bending stiffness of the external Restrained Units is partially reduced. For the three-layer truss simplified model, equilibrium equations can be formulated using the force method to analyze lateral deformation under arbitrary loading, from which the equivalent stiffness of the external Restrained Units can be derived. When a buckling-restrained brace (BRB) is subjected to compressive loading, the deformation mode of its core plate transitions gradually from a single-wave pattern to a multi-wave pattern, as illustrated in Fig. 4. This study focuses primarily on the stiffness variation of the core plate during its single-wave deformation stage. Guo Yanlin [20] developed a differential equation-based model for BRBs with four-channel steel composite restrained units and derived a simplified expression for the restrained stiffness. The key to this method lies in calculating the connection stiffness between restrained units. This analytical approach is also applicable to the SABRB with a straight core plate discussed in this paper.

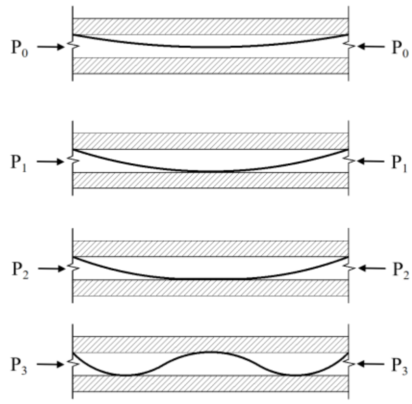

Fig. 4 Variation of core plate buckling modes

When the structure bends about the Y-axis, the sinusoidal lateral compressive force q_x exerted by the core plate on the external Restrained Units is calculated using the following expression [21–22]:

$$q_x = \pi^2 N\left(v_0 + g_x\right)\sin\left(\pi z / L\right) / L(1 - N / N_{crx} = \frac{\pi^2}{L^2} C_{qx} \sin\left(\pi z / L\right) \tag{1}$$

The concentrated lateral force V_{0x} exerted at the end of the units is calculated as follows:

$$V_{0x} = \frac{1}{2}\int_0^L q_x dz = \pi N\left(v_0 + g_x\right) / L\left(1 - N / N_{crx}\right) = C_{qx}\pi / L \tag{2}$$

Where, L is the length of the unit; v_0 is the initial imperfection value; N_{crx} is the overall buckling load of the inner core plate when bending about the x-axis; N is the axial force of the inner core plate; g_x is the unilateral gap value along the x-direction between the inner core plate and the peripheral restrained units; and C_{qx} is the maximum mid-span bending moment obtained from the second-order elastic analysis.

By establishing equilibrium equations based on the equivalent simplified model, the maximum lateral deformation under the action of lateral forces can be obtained. By comparing this with the maximum lateral deformation of an idealized unit with uniform stiffness subjected to the same lateral load, the equivalent lateral restrained stiffness of the external Restrained Units can be derived. If the stiffness of the web members is known, a simplified calculation method for the restrained stiffness can be derived using a modified version of the "continuous strut-tie model"—a model commonly applied to multi-branched reinforced concrete shear walls. In this approach, the web connections between the upper, middle, and lower chords are idealized as continuous elements [23].

When the units rotate about the Y-axis, two parameters are defined as follows:

$$\gamma_1 = 6 I_{2y} L^2 / \left(I_{cp} + I_{ud}\right) l_{bd} h_x \tag{3}$$

$$\gamma = 6I_{2y}L^2 / \left(I_{cp} + I_{ud}\right) l_{bd} h_x + 24 I_{2y} L^2 / A_{cp} l_{bd} h_x^3 \tag{4}$$

Let:

$$\lambda\left(\gamma, \gamma_1\right) = 4\gamma_1^2 / 4\gamma^2 + \pi^2 \tag{5}$$

Then, the stiffness reduction coefficient of the external Restrained Units is expressed as:

$$\mu_y = 1 \times 2\left(I_{ud} + I_{cp}\right) / \left[I_y \times 1 - \lambda\left(\gamma, \gamma_1\right)\right] \tag{6}$$

Where, I_y is the moment of inertia of the external Restrained Units as a whole about the Y-axis:

$$I_y = 2\left(I_{ud} + I_{cp}\right) + A_{cp} h_x^2 / 2 \tag{7}$$

3. Theoretical analysis of restrained coupling stiffness

3.1. Force analysis

The coupling stiffness of the external Restrained Units is jointly provided by the upper and lower restrained cover plates, the left and right lateral restrained units, and the bolts. It primarily reflects the unit's capacity to resist relative longitudinal sliding deformation between units. To investigate this, models with varying longitudinal dimensions of the restrained units were developed for analysis. Since the stiffening ribs on the lateral restrained units have a negligible influence on relative sliding deformation, and the segmentation of the lateral restrained units complicates stiffness evaluation, this section disregards the effects of stiffener placement and segmentation of the lateral restrained units. When the entire restrained unit bends about the Y-axis, a pair of equal and opposite forces is hypothetically applied at the neutral axis of the left and right lateral restrained units. This pair of unbalanced forces is transmitted from point A_1 on the left restrained to point B_1 on the right restrained via the following load path (see Fig. 5): starting from A_1, the force is transferred through the left flange, then via the bolts to the upper (or lower) restrained cover plate, then along the cover plate between bolts, through another bolt, and finally to the right lateral restrained and its flange, reaching B_1. The plates and bolts along this transmission path are idealized as web members, and their deformation directly influences the coupling stiffness of the restrained system.

The coupling stiffness can be further divided into two components: One part is provided by the in-plane stiffness of the restrained plates along the force transmission path. The other part stems from the out-of-plane bending stiffness, which is attributed to bolt rotation and longitudinal tilting during force transfer—this induces local out-of-plane deformation in the adjacent restrained plates.

3.2. Influence of in-plane plate stiffness on coupling stiffness

In the deformation calculation of the external Restrained Units, not all plates contribute to stiffness due to the discrete distribution of bolts. A numerical model of the buckling-restrained brace was established via ABAQUS, with an initial force applied about the Y-axis. In this study, the identical geometric and material parameters to those of the test specimen were adopted for model construction. The finite element model (FEM) accurately reproduced the geometric configuration of the bolts. In ABAQUS finite element analysis, the selection of solid element type and mesh size exerts a significant influence on the accuracy, computational efficiency, and stability of the model results. By reviewing the commonly used ABAQUS solid element types reported in relevant literature, this study compiled the findings in Table 1. Considering that the model involved in this paper requires extensive simulation of contact interactions, the C3D8R element is deemed the more suitable choice. The element size of the model is about 15 mm, as shown in Fig. 5(b). As revealed by the force analysis, during force transmission, only the bolts function as connecting units at the joint locations of the restrained units, while the plates immediately adjacent to the bolts do not provide any stiffness. However, for plates farther from the bolted joints, the area of the plates involved in load-bearing gradually increases; such regions are referred to as "effective plates." The effective zones of the upper/lower and left/right restrained units are illustrated in Fig. 5(a).

Table 1
Comparisons of different 3D element type

Type	Advantages	Disadvantages
C3D8: An 8-node linear brick.	Suitable for regular-shaped elements, enabling precise integration of polynomials within the stiffness matrix.	Risk of shear locking under bending loads, resulting in overestimated stiffness calculations.
C3D8R: An 8-node linear brick, reduced integration, hourglass control.	One fewer integration point per direction than fully integral elements, offering computational efficiency and superior adaptability to bending problems with reduced susceptibility to shear locking.	Sensitive to hourglass, potentially yielding excessively soft results.
C3D8I: An 8-node linear brick, incompatible modes.	Overcomes shear locking by introducing additional degrees of freedom, achieves accuracy close to quadratic elements, and has lower computational cost.	Sensitive to element distortion; unsuitable for contact analysis or large deformation problems.

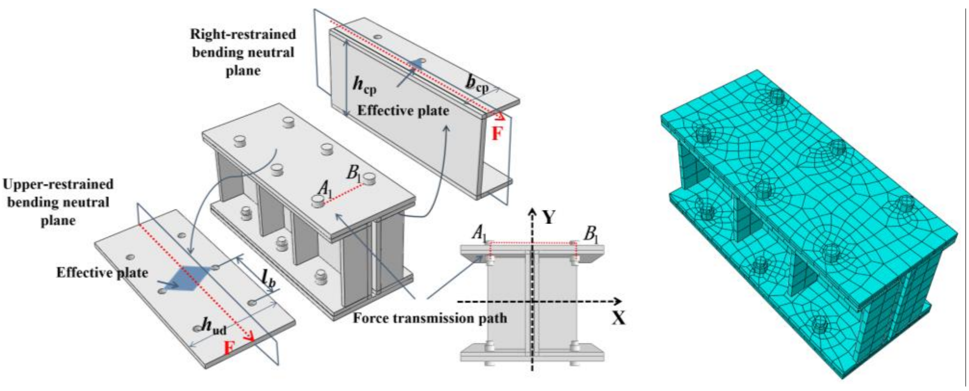

(a) Effective plate and force transfer paths (b) Mesh model

Fig. 5 Analysis model of SABRB

For the effective plate elements on the left (or right) restrained unit, the distance from the bolt center to the bending neutral axis of the left restrained unit is denoted as h_{cp}. It should be noted that within the range of the effective region, the distribution of the effective area is complex and difficult to define precisely. Accordingly, appropriate simplifications are employed in the subsequent calculations. The effective flange plate of the left restrained units is replaced by an equivalent strip with a uniform width, as illustrated in Fig. 5. This width is defined as the equivalent width, and its value is expressed as:

$$h_{cpy} = \alpha_{cp} \times b_{cp} \tag{8}$$

Where, α_{cp} is the effective width coefficient for the effective plate area on the left (or right) restrained unit.

Based on the force transmission path illustrated in Fig. 6, the load-transfer model can be simplified as a beam with one end pinned and the other end fixed. The pinned end corresponds to the bolted connection (i.e., the midpoint of the bolt shank), while the fixed end corresponds to the bending neutral axis of the plate, as illustrated in Fig. 5. The moment of inertia of this unit is:

$$I_{cp} = h_{cpy}^{3} t_{cpb} / 12 \tag{9}$$

Based on the simplified beam model, the longitudinal deformation Δ_{cp} induced by the longitudinal force F in the left (or right) restrained unit is expressed as [24]:

$$\Delta_{cp} = F h_{cp1}^{3} / 3EI_{cp} \tag{10}$$

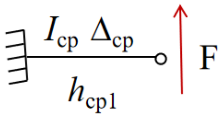

Fig. 6 Simplified force analysis of effective plates in left and right restrained units

The effective plate elements on the upper (or lower) restrained unit are analyzed using a similar approach. For the upper restrained unit, the distance from the bolt center to the bending neutral axis is denoted as b_{ud1}. By adopting the same modeling method applied to the left (or right) restrained unit, a simplified beam model is established, as illustrated in Fig. 7. In this model, the pinned end corresponds to the bolted connection, while the fixed end corresponds to the bending neutral axis of the upper restrained plate. The equivalent width and moment of inertia of the effective plate section are expressed as:

$$h_{udy} = \alpha_{ud} h_{ud} / 2 \tag{11}$$

$$I_{ud} = h_{udy}^{3} h_{ud} / 12 \tag{12}$$

Where, α_{ud} is the effective width coefficient for the upper (or lower) restrained unit.

According to this simplified model, the longitudinal deformation Δ_{ud} induced by the longitudinal force F in the upper (or lower) restrained unit is expressed as:

$$\Delta_{ud} = F h_{ud1}^{3} / 3EI_{ud} \tag{13}$$

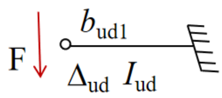

Fig. 7 Simplified force analysis of effective plates in upper and lower restrained units

Thus, the total in-plane deformation of the restrained plates is:

$$\Delta = \Delta_{ud} + \Delta_{cp} = F h_{cp1}^{3} / 3EI_{cp} + F h_{ud1}^{3} / 3EI_{ud} = F\delta_{y} \tag{14}$$

Where, δ_y is the coupling flexibility coefficient.

Through qualitative analysis of the effective plate area, it is found that the effective width coefficients α_{cp} and α_{ud} are influenced by the longitudinal bolt spacing l_{bd} and the distance from the bolt center to the bending neutral axis of the upper/lower and left/right restrained units. When the longitudinal bolt spacing decreases, the effective plate regions adjacent to neighboring bolts begin to overlap, thereby reducing the total effective area and resulting in a decrease in the effective width coefficient. Conversely, when the bolt spacing becomes sufficiently large, the effective width coefficient is no longer sensitive to changes in spacing. Similarly, when the distance from the bolt center to the bending neutral axis decreases, the spread of the effective plate area is limited, which also leads to a reduction in the effective width coefficient.

Table 2
Model parameters

Model	h_{cp}	t_{cp}	b_{cp}	t_{cpb}	h_{ud}	t_{ud}	h_{cp1}	b_{ud1}	l_{bd}
Model 1A	224	11.5	100	10	214	12	40	45	50-200
Model 1B	224	11.5	100	10	214	12	56	61	50-200
Model 1C	224	11.5	100	10	214	12	30-60	35-65	100
Model 1D	224	11.5	100	10	214	12	30-60	35-65	150
Model 2A	284	11.5	170	10	350	12	51	56	85-306
Model 2B	284	11.5	170	10	350	12	85	91	85-306
Model 2C	284	11.5	170	10	350	12	51-102	56-107	140
Model 2D	284	11.5	170	10	350	12	51-102	56-107	255
Model 3A	224	11.5	100	10	214	12	37.5	42.5	53.5-214
Model 3B	224	11.5	100	10	214	12	51	56	53.5-214
Model 3C	224	11.5	100	10	214	12	27.1-69.9	32.1-74.9	107
Model 3D	224	11.5	100	10	214	12	27.1-69.9	32.1-74.9	160.5
Model 4A	284	11.5	170	10	350	12	65	70	87.5-315
Model 4B	284	11.5	170	10	350	12	100	105	87.5-315
Model 4C	284	11.5	170	10	350	12	47.5-117	52.5-122	140
Model 4D	284	11.5	170	10	350	12	47.5-117	52.5-122	262.5
Model 5A	304	11.5	180	10	370	12	72	77	144-270
Model 5B	304	11.5	180	10	370	12	108	115	144-270
Model 5C	304	11.5	180	10	370	12	45-126	50-131	108
Model 5D	304	11.5	180	10	370	12	45-126	50-131	144
Model 5E	304	11.5	180	10	370	12	90	95	144-270

This study adopts a semi-analytical method combined with finite element analysis (FEA) to solve the effective width coefficient. Several configurations of external Restrained Units are designed by varying the bolt spacing (l_{bd}) and the bolt cross-sectional position (b_{ud1}). Corresponding finite element models are developed, with cross-sectional parameters summarized in the relevant Table 2. Contact relationships between the upper, lower, left, and right restrained units are defined. Assuming n groups of bolts are arranged longitudinally, a pair of opposing forces, F_1, is applied to the upper and lower restrained cover plates.

The force acting on each bolt group is thus $F=F_1/n$. Finite element analysis yields the relative displacement Δ_x between the upper and lower neutral axes. The flexibility coefficient of the bolted connection can therefore be expressed as: $\delta_x=\Delta_x/F$. This coefficient is then used to evaluate the corresponding stiffness and effective width coefficients. To determine the effective width coefficient α_{cp} for the left and right restrained units, a pair of equal and opposite longitudinal forces is applied along the cut edges at the bending neutral axis of the left and right restrained units. The resulting longitudinal displacement of nodes on these edges is recorded. To ensure that the computed displacement exclusively represents the deformation of the lateral restraints, the upper and lower restrained cover plates are modeled as rigid bodies.

3.2.1. Determination of the coefficient α_{cp}.

Two coefficients, α_{cp1} and α_{cp2}, are defined to respectively represent the effects of longitudinal bolt spacing l_{bd} and the bolt's cross-sectional position h_{cp1}, and they are expressed as:

$$\alpha_{cp1}=l_{bd}/b_{cp} \tag{15}$$

$$\alpha_{cp2}=h_{cp1}/b_{cp} \tag{16}$$

The analytical expressions show that the value of the effective width coefficient α_{cp} depends solely on these two factors, and the influencing factors are independent of each other. Thus, α_{cp} can be derived by multiplying the two individual influence coefficients, expressed as:

$$\alpha_{cp}=\alpha^{l}_{cp1}\alpha^{s}_{cp2} \tag{17}$$

Where, α^{l}_{cp1} represents the influence factor associated with the longitudinal bolt spacing l_{bd}, and α^{s}_{cp2} denotes the influence factor associated with the bolt's cross-sectional position h_{cp1}.

The relationship between the coefficient α^{l}_{cp1} and the parameter α_{cp} obtained from the finite element results is illustrated in the corresponding Fig. 8. As the bolt spacing increases, the value of α_{cp} remains relatively stable, which is consistent with the earlier qualitative analysis. The relationship between α^{s}_{cp2} and α_{cp} is presented in Fig. 8, showing an approximately linear trend. Through curve fitting, the expressions for these two influence factors can be derived as follows:

$$\alpha_{cp}=\left\{-0.0457\left(\alpha_{cp1}\right)^2+0.1361\alpha_{cp1}+0.5209\right\}(1.3095\alpha_{cp2}+0.0284) \tag{18}$$

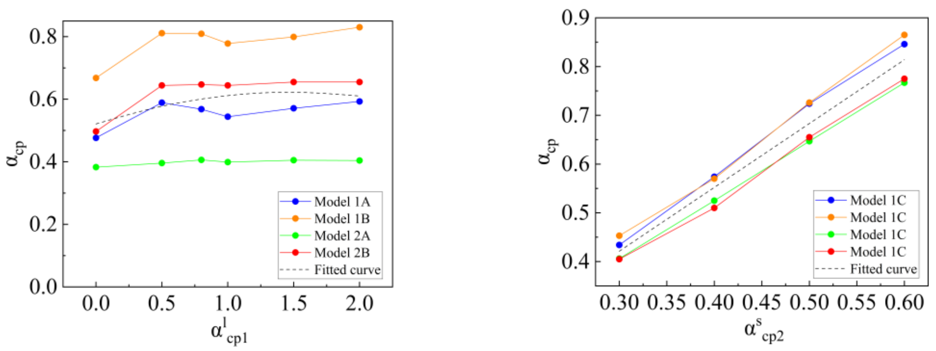

(a) Varying the bolt spacing (b) Varying the bolt cross-sectional position

Fig. 8 Fitting calculation of the coefficient α_{cp}

3.2.2. Determination of the coefficient α_{ud}

Similarly, two coefficients, α_{ud1} and α_{ud2}, are defined to account for the effects of the bolt spacing l_{bd} and the bolt's cross-sectional position b_{ud1}, respectively, and are expressed as:

$$\alpha_{ud1}=2l_{bd}/h_{ud} \tag{19}$$

$$\alpha_{ud2}=2b_{ud1}/h_{ud} \tag{20}$$

The relationships between these two parameters and the coefficient α_{ud} are illustrated in Fig. 8. The fitted equations for the parameters and the coefficient α_{ud} are given as follows:

$$\alpha_{ud}=\left\{-0.1616\left(\alpha_{ud1}\right)^2+0.4407\alpha_{ud1}+0.1707\right\}(0.8935\alpha_{ud2}+0.0079) \tag{21}$$

Where, α^{l}_{ud1} denotes the influence factor associated with the longitudinal bolt spacing $l_{bd,}$ and α^{s}_{ud2} represents the influence factor related to the bolt's cross-sectional position b_{ud1}.

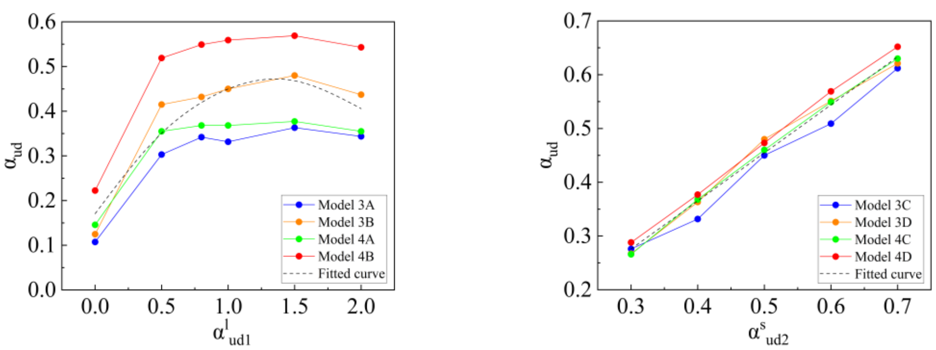

(a) Varying the bolt spacing (b) Varying the bolt cross-sectional position

Fig. 9 Fitting calculation of the coefficient α_{ud}

3.3. Coupling stiffness associated with the out-of-plane stiffness of restrained plates

The upper and lower restrained cover plates are connected to the left and right restrained units via bolts. Due to bolt deformation, rotational displacement occurs between the mid-planes of these units, accompanied by longitudinal displacement; these combined effects result in a reduction in the overall stiffness of the external Restrained Units. Given the complex interaction between the connected plates, a correction factor is introduced to the previously derived stiffness of the external Restrained Units to account for the influence of rotational deformation. This correction further refines the analysis of factors affecting the stiffness of the SABRB external Restrained Units.

To incorporate the effects of rotational deformation, the finite element model is enhanced by introducing out-of-plane restraints between the upper/lower cover plates and the flanges of the left/right restrained units. By comparing the relative sliding deformation Δ obtained from this improved model with the Δ derived in Section 2.2, the stiffness reduction coefficient due to rotational deformation, denoted as μ_{0y}, can be determined.

Two parameters are defined: α_{01}, which represents the influence of bolt spacing on the reduction coefficient μ_{0y}, and α_{02}, which represents the influence of the bolt's cross-sectional position on μ_{0y}. The effects of these parameters are illustrated in Fig. 10. Based on the data points presented in Fig. 10(a), a fitted expression describing the influence of variations in bolt spacing on the reduction coefficient is derived as:

$$\mu_{0y} = 0.0402\alpha_{01}^2 - 0.116\alpha_{01} + 0.9833 \tag{22}$$

As shown in Fig. 10(b), although the bolt's cross-sectional position influences the reduction coefficient, the variation is relatively small and generally remains around 0.9. Thus, the corresponding fitted expression for the reduction coefficient is:

$$\mu_{0y} = 0.9\left(0.0402\alpha_{01}^2 - 0.116\alpha_{01} + 0.9833\right) \tag{23}$$

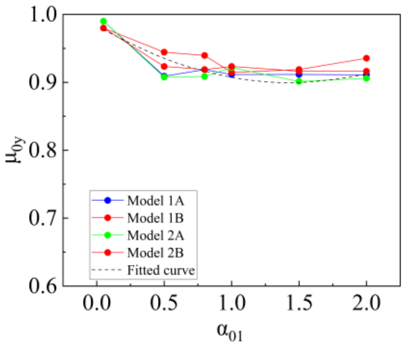

(a) Varying the bolt spacing

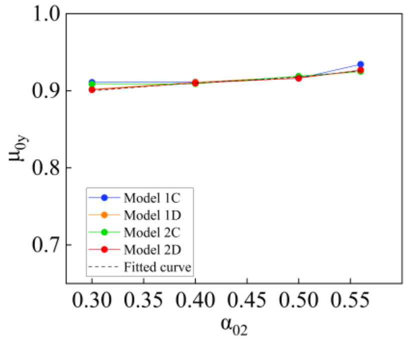

(b) Varying the bolt cross-sectional position

Fig. 10 Calculation of the reduction coefficient μ_{0y}

3.4. Determination of restrained stiffness

Considering the influence of out-of-plane deformation of the restrained plates, Equation (14) should be revised as:

$$\Delta = F\delta_y / \mu_{oy} \tag{24}$$

If the longitudinal deformation is calculated using the simplified model illustrated in Fig. 3, then:

$$\Delta = Fh_x^3 / 48EI_{by} \tag{25}$$

By comparing the two expressions, the expression for EI_{2y} can be derived as:

$$EI_{by} = \frac{0.9\left(0.0402\alpha_{01}^2 - 0.116\alpha_{01} + 0.9833\right)h_x^3}{48\left(\dfrac{h_{cp1}^3}{3EI_{cp}} + \dfrac{h_{ud1}^3}{3EI_{ud}}\right)} \tag{26}$$

The stiffness of the restrained units can thus be expressed as $\mu_y EI$, where I is the composite moment of inertia of the external Restrained Units, calculated under the assumption of full composite action based on the plane section hypothesis.

4. Finite element analysis verification of the stiffness reduction coefficient for the external restrained units

4.1. Example verification of the stiffness reduction coefficient

To verify the accuracy of the theoretical formula derived in the previous section, a numerical case study is executed. The Model 5 series listed in Table 2 is chosen for validation. With both ends of the SABRB assumed to be pinned, a sinusoidally distributed load is imposed on the left and right restrained units. The resulting displacements under varying bolt cross-sectional positions and bolt spacings are analyzed and then compared with those of a monolithic BRB under the same loading conditions. From this comparison, the stiffness reduction coefficient of the segmented external Restrained Units is deduced, which is subsequently compared with the theoretical coefficient derived earlier. The displacement of a monolithic BRB under the same loading condition can be calculated using the following formula:

$$\Delta = q_s L^4 / \pi^4 EI \tag{27}$$

Where, I is the composite moment of inertia of the external Restrained Units assuming full composite action, calculated based on the plane section hypothesis, and L is the length of the BRB.

The stiffness reduction coefficients obtained from the simplified calculation formula and finite element analysis (FEA) are both presented in Fig. 11. As illustrated in Fig.11(a)、(c), despite minor discrepancies between the two sets of results, the calculation error does not exceed 10%, and the overall trend is consistent. To more intuitively demonstrate the minimal discrepancy between the results derived from the calculation formulas and those obtained via finite element analysis, a bar chart for result comparison was added to facilitate a more straightforward understanding of the accuracy of the calculation formulas, as illustrated in Fig. 11(b) and 11(d). It is noteworthy that for very short BRB specimens with large bolt spacing, the calculated stiffness reduction coefficient may be significantly low, which does not reflect practical behavior. However, when bolts are arranged with sufficient density, the simplified formula yields conservative results, thereby enhancing safety. Therefore, using the simplified formula to estimate the stiffness of the external Restrained Units in BRBs is considered reasonable and practical.

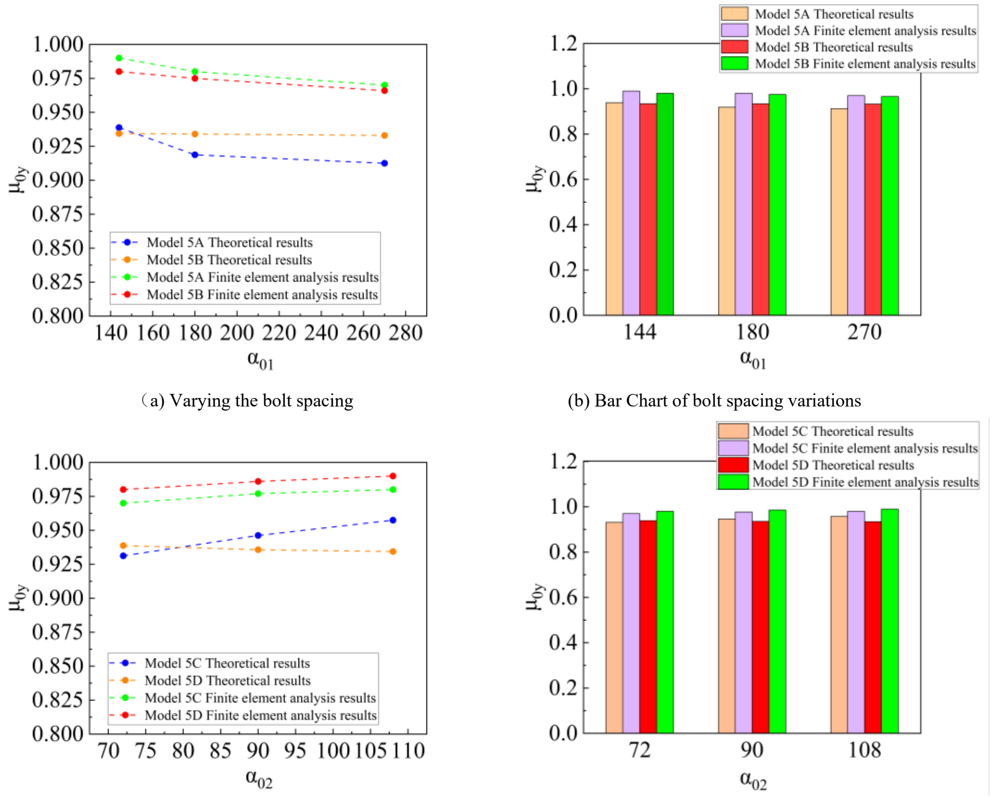

(a) Varying the bolt spacing (b) Bar Chart of bolt spacing variations

(c) Varying the bolt spacing (d) Bar Chart of bolt section position variations

Fig. 11 Comparison between the simplified theoretical formula results of μ_{0y} and the calculation results of the finite element analysis

4.2. Analysis of Factors influencing the stiffness of the external restrained units

In the novel SABRB, the external Restrained Units incorporate transverse stiffening ribs, with the lateral restrained units adopting a segmented configuration. These design features exert a significant influence on the overall stiffness of the external restrained units. To examine this influence, the parameters of Model 5A, 5C, 5D, and 5E are modified to generate Model 5F1~3, 5G1-3, 5H1-3, and 5J1-3, respectively, as summarized in Table 3.

The transverse stiffening ribs are designed with a thickness identical to that of the flanges of the left and right restrained units, and a width equal to half the flange width. In the proposed model, the left and right restrained units are divided into three segments, which are aligned with the positions of the limiting plates on the inner core plate to optimize material utilization. Given that this study focuses primarily on the stiffness of the external Restrained Units, the lengths of these three segments are adjusted accordingly when bolt spacing is varied—this adjustment not only reflects practical restraints but also more accurately captures how segmentation influences stiffness. A sinusoidally distributed load is applied to the left and right restrained units to compute the mid-span displacement of the external Restrained Units. These displacements are then compared with those from unmodified models to assess the impacts of lateral restrained segmentation and stiffening rib configuration on stiffness. The spacing of the transverse stiffening ribs is set to 0.6 times the height h_{cp} of the SABRB. In numerical simulations, by varying the bolt spacing and cross-sectional position, changes in the displacement of the external Restrained Units are recorded—these changes, as illustrated in Fig. 12, directly reflect variations in restrained stiffness. Finite element results reveal that segmenting the left and right restrained units, coupled with the addition of transverse stiffeners, effectively reduces the mid-span displacement of the SABRB external Restrained Units—an indication of increased stiffness. Specifically, when the rib spacing is set to $0.6h_{cp}$, the displacement is significantly smaller than in the unmodified model. As shown in Fig. 12, variations in bolt spacing and cross-sectional position lead to only minor displacement changes, with correspondingly limited variations in stiffness. For the models in Table 3 that share the same letter but different numbers, the differences arise from the adjustment of bolt parameters or bolt cross-sectional positions. Therefore, these models are not labeled individually in Fig. 12, but are represented by the same corresponding letter.

Table 3
Parameter table for different models of external restrained units

Model	h_{cp}	t_{cp}	b_{cp}	t_{cpb}	h_{ud}	t_{ud}	h_{cp1}	b_{ud1}	l_{bd}
Model 5F1	304	11.5	180	10	370	12	72	77	144
Model 5F2	304	11.5	180	10	370	12	72	77	180
Model 5F3	304	11.5	180	10	370	12	72	77	270
Model 5G1	304	11.5	180	10	370	12	72	77	108
Model 5G2	304	11.5	180	10	370	12	90	95	108
Model 5G3	304	11.5	180	10	370	12	108	113	108
Model 5H1	304	11.5	180	10	370	12	72	77	144
Model 5H2	304	11.5	180	10	370	12	90	95	144
Model 5H3	304	11.5	180	10	370	12	108	113	144
Model 5J1	304	11.5	180	10	370	12	90	95	144
Model 5J2	304	11.5	180	10	370	12	90	95	180
Model 5J3	304	11.5	180	10	370	12	90	95	270

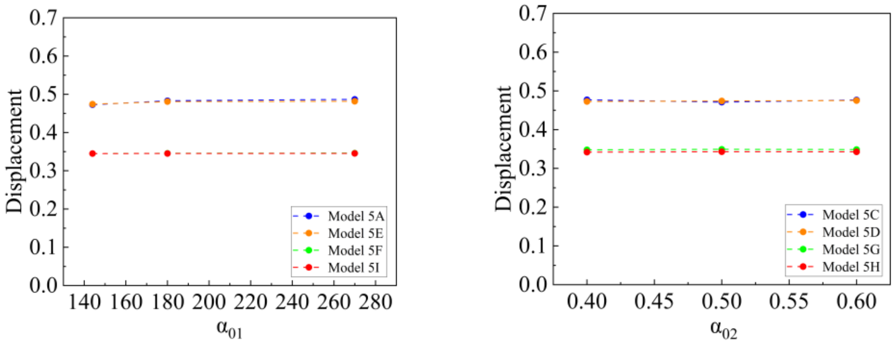

(a) Varying the bolt spacing (b) Varying the bolt cross-sectional position

Fig. 12 Influence of discontinuous lateral restrained units and transverse stiffeners on external restrained stiffness

To more distinctly demonstrate the discrepancy between the stiffness calculation formula derived in this paper and the results obtained via the conventional method, the bending stiffness of Model 5A and Model 5E was calculated using both approaches, as shown in Fig. 13,the discrepancy between the flexural rigidity of the buckling-restrained brace calculated by the simplified method and that derived from the theoretical formula proposed in this paper reaches 29.3%.

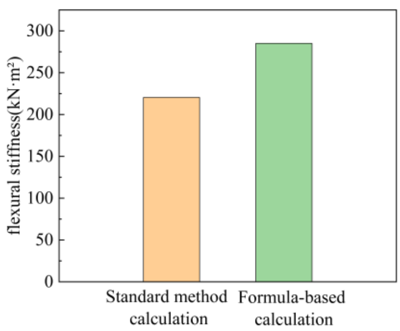

Fig. 13 Comparison of bending stiffness calculated by different methods

Table 4
Correction coefficient

Model	**correction coefficient α**
5F1	1.37
5F2	1.37
5F3	1.382
5G1	1.374
5G2	1.398
5G3	1.348
5H1	1.382
5H2	1.393
5H3	1.406
5J1	1.367
5J2	1.396
5J3	1.394

The model correction coefficient a is derived by comparing the stiffness of the models in Table 4 with that of the baseline model, and the specific values are presented in Table 4. It is assumed that the values of the correction coefficient α obey a normal distribution, and the lower limit of the 99.5% confidence interval is adopted. In this case, a can be expressed as [25]:

$$\alpha=\alpha_{m}-t_{0.05}(n_{0}-1)S/\sqrt{n_{0}} \tag{28}$$

where, α_m is the average of α; n_0 is the number of specimens; S is the sample standard deviation; $t_{0.05}(n_0\text{-}1)$ is the value of t distribution. α is calculated according to equation (28) and Table 4, whose value equals to 1.382. Thus, the suggest value of α is simplified to be 1.38.

Consequently, when the left and right restrained units are segmented by practical design requirements and stiffening ribs are arranged at 0.6 times the unit height, the stiffness of the peripheral constrained unit should be amplified by a factor of 1.38. Specifically, the bending stiffness of the buckling-restrained brace calculated by the conventional method is 220.5 kN·m², while that of the segmented assembled buckling-restrained brace calculated by the theoretical formula proposed herein is 285.1 kN·m². The result of the proposed method deviates by 29.3% from that of the conventional method, indicating a significant difference. This verifies that the stiffness calculation formula derived in this study exhibits substantial guiding significance for the design of this type of buckling-restrained brace.

The flow for calculating the external restraining stiffness of this type of buckling-restrained brace using theoretically derived formulas is illustrated in Fig. 14.

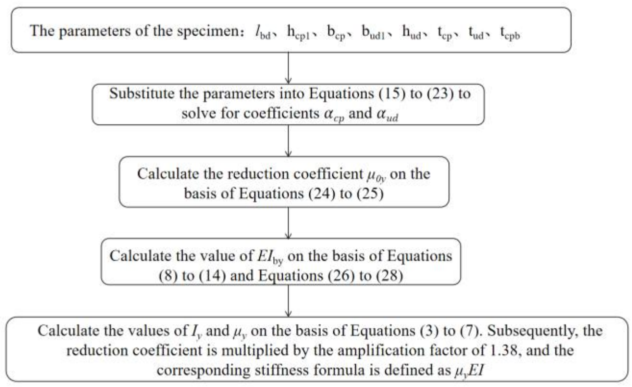

Fig. 14 Calculation process for stiffness of external restraint units of SABRB

5. Experimental validation

5.1. Compression test of external restraining units

To further verify the rationality of the theoretical derivation formulas in this paper, experiments are now carried out for verification. Q235 steel is used to fabricate the specimen of the externally restrained units of the SABRB, as shown in Figs. 15 and 16. Since the actual and simulated force-bearing positions of the external restrained units are internal, to better reflect the actual situation, half of the lateral restrained units are assembled in the experiment. The specimen is placed on the hinged support, and a mass plate is placed inside. The total mass of the mass plate is 30kg. A sinusoidal loading is simulated, and the loading diagram is shown in Fig. 17. A hydraulic device is used for loading, as shown in Fig. 18. To fully exploit the material properties, the loading speed is controlled at 2mm/min throughout the process to obtain the ultimate bearing capacity of the external restrained units. Then, its flexural stiffness is calculated and compared with the restrained stiffness obtained from the theoretical derivation formulas in this paper.

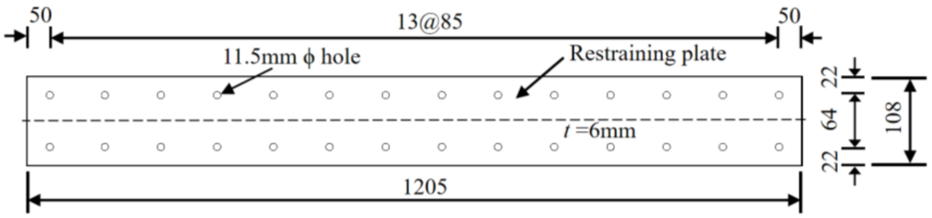

(a) Upper and lower restrained cover plates

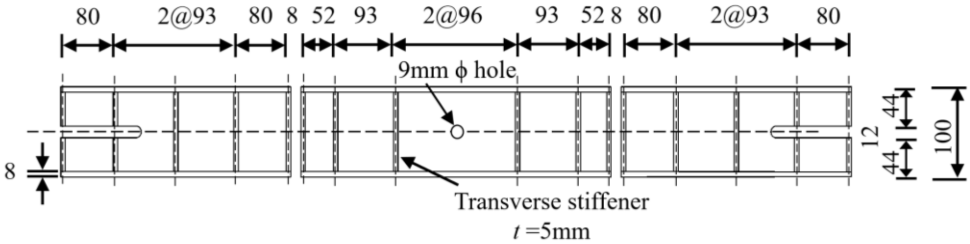

(b) Left and right restrained units

Fig. 15 Dimension of specimen

Fig. 16 Specimen installation

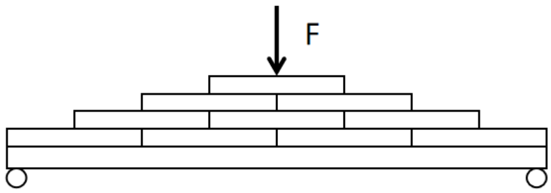

Fig. 17 Schematic diagram of loading

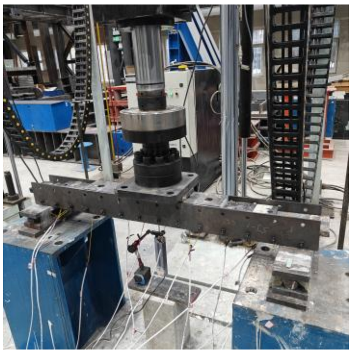

Fig. 18 Hydraulic loading

The load-displacement curve of the external restrained units of the SABRB throughout the entire loading process is shown in Fig. 20(a). The ultimate load in the elastic stage, as illustrated in Fig. 20(b), corresponds to a displacement of 20.01 mm and a bearing capacity of 187.63 kN. Using the theoretical derivation formula in this paper, the flexural stiffness of the externally restrained units is calculated as 165.7 kN·m². The formula for the maximum mid-span deflection is as follows：

$$v = 5ql^4 / 384EI \tag{29}$$

Substituting the values and simplifying, the actual experimental flexural stiffness EI is determined to be 143.3 kN·m². During the test, strain gauges were evenly attached to the left and right restrained units. To better illustrate the deformation behavior, data from the middle strain gauges N_1 and N_2 are presented as representative, as shown in Fig. 19. From the test data in Fig. 23, it is evident that the strain at location N_1 reached only 570 με, and that at location N_2 reached only 350 με. As the loading displacement increased, the specimen underwent global buckling accompanied by significant local deformation, and the test was terminated immediately, as shown in Figs. 21、22. The error between the theoretically derived formula and the experimentally obtained flexural stiffness is 14.8%, which is relatively small, indicating a relatively low error level. This indicates that the theoretical framework proposed in this paper aligns well with actual stress conditions, providing robust support for calculating the stiffness of the external Restrained Units of BRBs and laying a theoretical foundation for subsequent research.

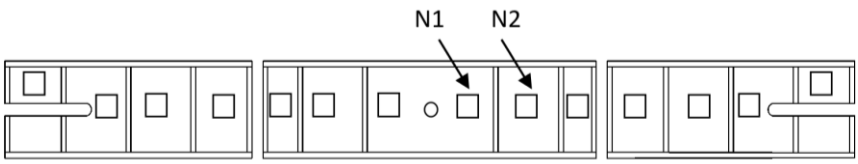

Fig. 19 Strain gauge layout

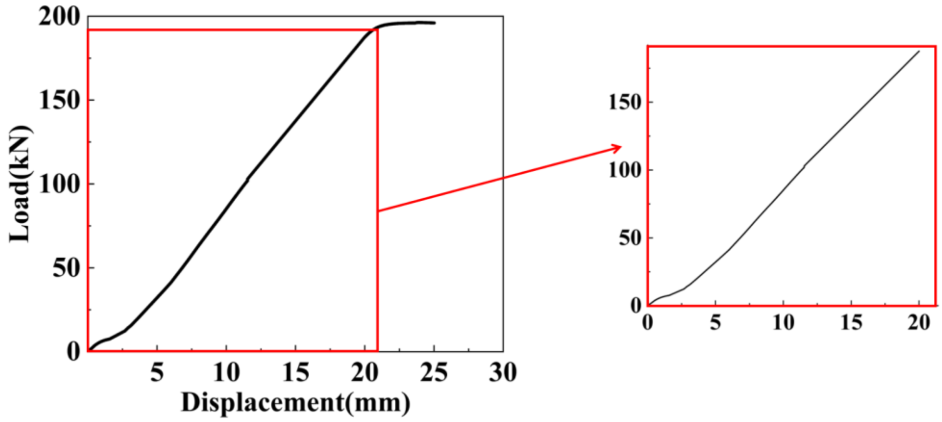

(a) The full-range load-displacement curve (b) The elastic-stage load-displacement curve

Fig. 20 The load-displacement curve

Fig. 21 The global buckling

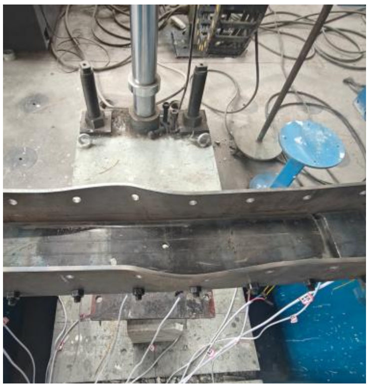

Fig. 22 The local deformation

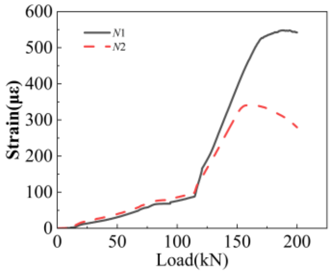

Fig. 23 Strain-load curve

5.2. Overall axial compression test

To further validate the flexural stiffness of the external restraining components of this assembled buckling-restrained brace, a full-scale axial compression test was performed. The fabrication details of the test specimen are presented in Figure 24. Both the core plate and restrained units were fabricated from Q235 steel.

A servo-hydraulic actuator was adopted as the test loading device to apply cyclic loads to the specimen, which was firmly mounted on a rigid loading frame to ensure the stability of the brace. The SABRB was connected to the floor beam in the structural assembly, and the overall installation configuration is detailed in Fig. 25. The test adopted a tension-first-then-compression loading protocol, and the loading regime of the specimen is presented in the table 5. When the displacement was loaded to 31.2 mm (1/50 of the brace length) and the third loading cycle was initiated, brittle fracture occurred in the region of the core plate end without lateral restraint units. The forward loading was immediately terminated, and an attempt was made to apply reverse compression; however, the specimen had already completely lost its load-bearing capacity, and the test was officially concluded. The external restraint units maintained elastic deformation throughout the entire test process. The final failure mode of the brace is detailed in Fig. 26.

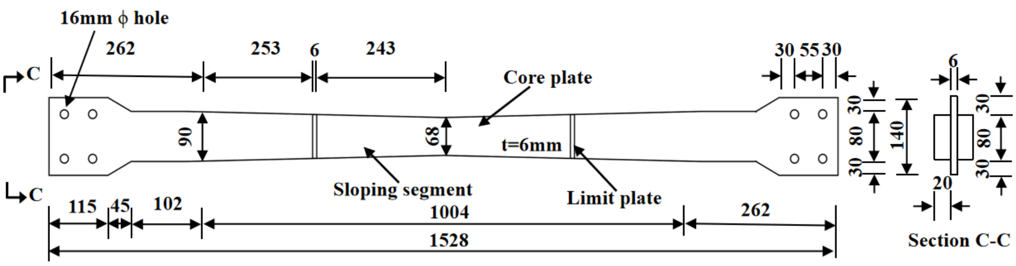

(a) Core plate

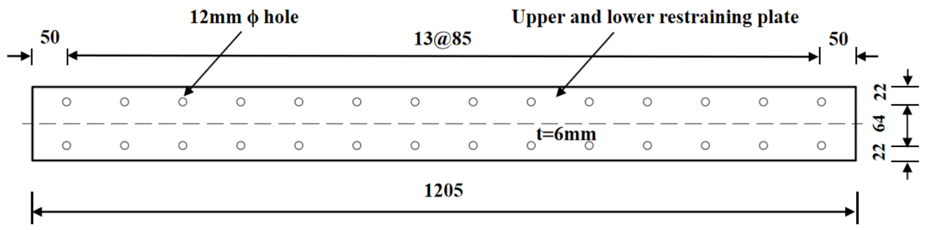

(b) Upper and lower restrained cover plates

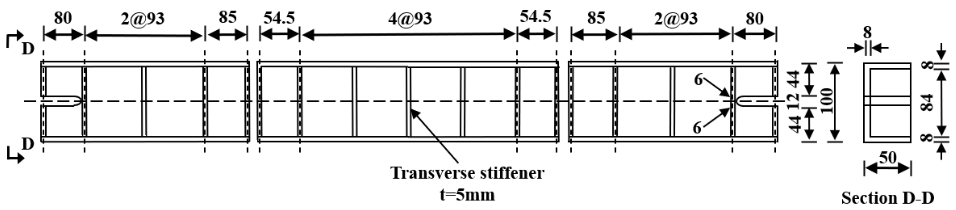

(c) Left and right restrained units

Fig. 24 Machining dimension drawing of units

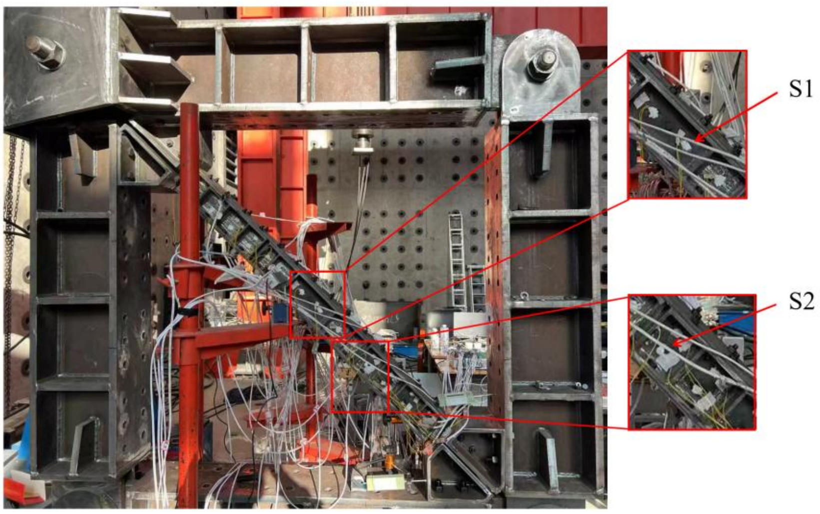

Fig. 25 Test setup of SABRB

Table 5
Loading system

Structural height（mm）	Axial strain	Displacement Amplitude（mm）	Loading Cycles
	1/300	6.24	3
	1/200	7.8	3
1560	1/150	10.4	3
	1/100	15.6	3
	1/50	31.2	3

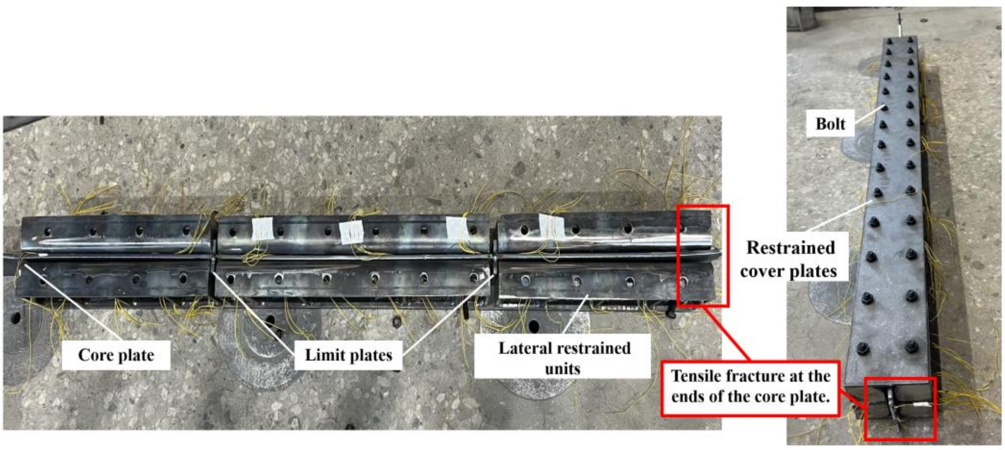

Fig. 26 Specimen failure

To measure the variations in the external restraining components during the test, strain gauges were uniformly affixed to them. For better illustration of their deformation characteristics, S1 and S2 were selected as typical measurement points, as shown in Fig. 25. As can be seen from Fig. 27, the strains of S1 and S2 were obtained. For Q235 steel, its yield strain ε_y was calculated by the formula $\varepsilon_y = f_y / E$, resulting in $\varepsilon_y = 235/210000 = 1.119\times10^{-3}$, equivalent to 1119 $\mu\varepsilon$. Throughout the loading process, the external restrained units remained in an elastic state, with their strains consistently lower than the yield strain. Therefore, it can be concluded that the external restraining components were capable of effectively resisting the lateral pressure exerted by the core plate and restricting the deformation of the core plate during the entire axial loading process, thus ensuring the normal operation of the assembled buckling-restrained brace.

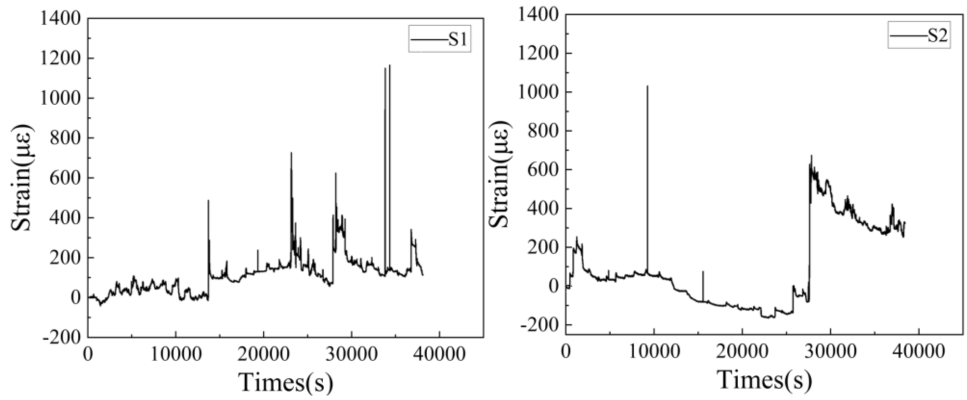

(a) (b)

Fig. 27 Strain during loading process

6. Conclusions

This paper investigates the mechanism and stiffness of the external Restrained Units in an SABRB. Since the restrained units are bolt-connected, the load-bearing behavior of the external restrained units in SABRBs differs from that in integral BRBs, with corresponding variations in the stiffness of the external restrained units. Based on a simplified truss model, this paper derives and fits a formula for calculating the stiffness reduction coefficient of the external restrained units through an analysis of its load-bearing mechanism and numerical simulations. The formula incorporates the influences of bolt spacing and bolt cross-sectional position, and its rationality is verified via numerical analyses. Additionally, the segmentation of left and right restrained units and the arrangement of transverse stiffeners can also induce changes in the stiffness of the external restrained units. Through comparisons of numerical simulation data, a reasonable layout scheme for transverse stiffeners is determined: when transverse stiffeners are arranged at 0.6 times the height of the external restrained units, the stiffness of the external restrained units in SABRBs can match that of integral BRBs. This study provides a stiffness reduction coefficient, proposes a formula for calculating the flexural stiffness of the external restrained units, and further validates the stiffness theory presented in this paper through experiments.

Funding

This research was funded by the Science and Technology Development Plan Project of Jilin Province, China, grant number: YDZJ202401594ZYTS.

The definitions of all parameter symbols adopted in this study are presented in Nomenclature.

Nomenclature	
h_{ud}	the width of the upper (and lower) restrained cover plates
t_{ud}	the thickness of the upper (and lower) restrained cover plates
h_{cp}	the height of the left (and right) lateral restrained units
t_{cp}	the thickness of the web plate of the left (and right) lateral restrained units
b_{cp}	the flange width of the left (and right) restrained units
t_{cpb}	the flange thickness of the left (and right) restrained units
h_{cp1}	the distance from the bolt center to the neutral axis of the flange
b_{ud1}	the distance from the bolt center to the mid-plane of the upper (and lower) restrained cover plates
h_x	the distance between the neutral axes of the left and right restrained units
EI_{cpy}	the bending stiffness of the left (and right) restrained units
A_{cp}	the cross-sectional area of the left (and right) restrained units
EI_{udy}	the bending stiffness of the upper (and lower) restrained cover plates
A_{ud}	the cross-sectional area of the upper (and lower) restrained cover plates
l_{bd}	the spacing between web members corresponds to the distance between adjacent bolts
EI_{by}	the bending stiffness of the web members
q_x	the sinusoidal lateral compressive force
L	the length of the unit?
v_0	the initial imperfection value
N	the axial force of the inner core plate
N_{crx}	the overall buckling load of the inner core plate
g_x	the unilateral gap value along the x-direction between the inner core plate and the peripheral restrained units

C_{qx}	the maximum mid-span bending moment obtained from the second-order elastic analysis
V_{0x}	the concentrated lateral force V_{0x} exerted at the end of the units
γ_1	the parameters related to the stiffness reduction coefficient are defined
I_{cp}	the force transfer model of the left (and right) restrained units is simplified as the moment of inertia of the member
I_{ud}	the force transfer model of the upper (and lower) restrained cover plates is simplified as the moment of inertia of the member
γ	the parameters related to the stiffness reduction coefficient are defined
μ_y	the stiffness reduction coefficient of the external Restrained Units
I_y	the moment of inertia of the external Restrained Units as a whole about the Y-axis
h_{cpy}	the effective plate width of the left (and right) restrained units
α_{cp}	the effective width coefficient for the effective plate area on the left (or right) restrained units
Δ_{cp}	the longitudinal deformation induced by the longitudinal force F in the left (or right) restrained units
h_{udy}	the effective plate width of the upper (and lower) restrained cover plates
α_{ud}	the effective width coefficient for the effective plate area on the upper (or lower) restrained cover plates
Δ_{ud}	the longitudinal deformation induced by the longitudinal force F in the upper (or lower) restrained cover plates
Δ	the total in-plane deformation of the restrained plates $\Delta=\Delta_{ud}+\Delta_{cp}$
δ_y	the coupling flexibility coefficient
F	a pair of opposing forces
F_1	the force acting on each bolt group
δ_x	the flexibility coefficient of the bolted connection
l_{bd}	the longitudinal bolt spacing
α_{cp1}	the coefficient for the effect of longitudinal bolt spacing on the left (and right) restrained units
α_{cp2}	the coefficient for the effect of bolt section position on the left (and right) restrained units
α^{l}_{cp1}	the influence factor of the left (and right) restrained units considering the effect of longitudinal bolt spacing l_{bd}
α^{s}_{cp2}	the influence factor of the left (and right) restrained units considering the effect of bolt section position h_{cp1}
α_{ud1}	the coefficient for the effect of longitudinal bolt spacing on the upper (and lower) cover plates
α_{ud2}	the coefficient for the effect of bolt section position on the upper (and lower) cover plates
α^{l}_{ud1}	the influence factor of the upper (and lower) cover plates considering the effect of longitudinal bolt spacing l_{bd}
α^{s}_{ud2}	the influence factor of the upper (and lower) cover plates considering the effect of bolt section position b_{ud1}
μ_{0y}	the stiffness reduction coefficient due to rotational deformation
α_{01}	the influence of bolt spacing on the reduction coefficient μ_{0y}
α_{02}	the influence of the bolt's cross-sectional position on μ_{0y}
v	the maximum mid-span deflection

References

[1] S.S. Cui, Y. Chen, J.C. Mwizerwa, W.H. Chen, Y.Z. Chen, Seismic performance of precast concrete frames with buckling-restrained braces, J. Earthq. Eng. 27 (7) (2023) 1920-1942.

[2] H.H. Dong, X.L. Du, Q. Han, K.M. Bi, H. Hao, Hysteretic performance of RC double-column bridge piers with self-centering buckling-restrained braces, B. Earthq. Eng. 17 (6) (2019) 3255-3281.

[3] X.N. Wei, B. Michel, Analytical investigation of buckling restrained braces' applications in bidirectional ductile end diaphragms for seismic performance of slab-on-girder bridge, Eng. Struct. 141 (2017) 634-650.

[4] J.K. Lu, Y. Ding, B. Wu, Y.Y. Li, J.X. Zhang, Experimental study of buckling-restrained brace with longitudinally profiled steel core, Struct. Eng. Mech. 81 (16) (2022) 715-728.

[5] Z. Yun, Y.S. Cao, T. Jiro, G.Q. Zhong, Z.M. He, Experimental and numerical investigation of a novel all-steel assembled core-perforated buckling-restrained brace, J. Constr. Steel. Res. 193 (2022).

[6] L.J. JIA, H.B. Ge, P. Xiang, Y. Liu, Seismic performance of fish-bone shaped buckling-restrained braces with controlled damage process, Eng. Struct. 169 (15) (2018) 141-153.

[7] Y.L. Guo, J.Z. Tong, X.A. WANG, P. Zhou, Subassemblage tests and design of steel channels assembled buckling-restrained braces, B. Earthq. Eng. 16 (9) (2018) 4191-4224.

[8] Y.L. Guo, B.H. Zhang, B.L. Zhu, P. Zhou, Y.H. Zhang, J.Z. Tong, Theoretical and experimental studies of battened buckling-restrained braces, Eng. Struct. 136 (2017) 312-328.

[9] Y.L. Guo, B.H. Zhang, X. A. Wang, Z.Q. Jiang, Research progress on design theory of assembled buckling-restrained brace, JACE. 30 (1) (2013) 1-12.

[10] C. Zeng, Y.F. Zhang, G.S. Xu, T. Wang, T.L. Pan, D.H. Wang, Quasi-static cyclic tests on the hysteretic behavior of buckling-restrained bracs with a T-sectioncoe, Eng. Mech. 38 (9) (2021) 124-132, 181.

[11] C. Fang, W. Wang, C.X. Qiu, S.L. Hu, G.A. Macrae, M.R. Eatherton, Seismic resilient steel structures: A review of research, practice, challenges and opportunities, J. Constr. Steel. Res. 191 (2022) 107172-107172.

[12] Y.L. Li, Y.X. Zhang, C.Y. Xiao, B.L. Wu, B.W. Jin, Performance study of eccentrically braced steel frames with core tube flange connection, J. Constr. Steel. Res. 216 (2024).

[13] X.C. Duan. Z.X. Zeng, X Liu, Y. Luo, Y.H. Ma, Experimental and numerical study of locking steel plate damper for seismic resistance, J. Constr. Steel. Res. 218 (2024).

[14] A.L. Zhang, J. Liu, Z.Q. Jiang, K. Guo, S.J. Su, Seismic performance evaluation of steel frame-support structures embedded with double-stage prefabricated buckling-restrained braces. Ind. Constr. 53 (9) (2023) 54-61.

[15] C.G. Li, Z.Y. Wang, H.D. Yan, Hysteresis performance test of all angle steel constraint and aluminum alloy plate assembled buckling-restrained braces, China Civil Engineering Journal. (2023) 1-12.

[16] S. Xu, Y. Li, X. L. Wang, A fully bolted buckling-restrained brace, 2022-02-01, CN202122141810.7.

[17] W. Guo, J.Z. Li, N.L. Xiang, Seismic performance of the buckling-restrained brace central buckle for long-span suspension bridges, J. Earthqu. Tsunami. 12 (5) (2018).

[18] K. Inoue, S. Sawaisumi, H.B. Yasuo, Bracing design criterion of the reinforced concrete panel including unbonded steel diagonal braces, J. Struct. Constr. Eng. 432 (5) (1992) 41—49.

[19] N. T, S. Takahashi. A study on the elasto-plastic behavior of unbonded composite bracing (Part 2: analytical studies), J. Struct. Constr. Eng. 422 (4) (1991) 45—56.

[20] X.A. Wang, Y.L. Guo, Z.Q. Jiang, B.H. Zhang, Study on restraining mechanism and stiffness of a four-channel assembled steel buckling-restrained brace, Prog. Steel Build. Struct. 15 (03) (2013) 1-11+47.

[21] Y.L. Guo, X.A. Wang, L.X. Jang, Design Theory of Assembled Buckling-Restrained Braces and Buckling-Restrained Braced Frames, Struct Eng. 26 (6) (2010) 164-176.

[22] Y.L. Guo, L.X.Jiang, Behavior and application of buckling-restrained braces assembled with section steels, Build. Struct. 40 (1) (2010) 30-37.

[23] Y.L. Guo, X.A. Wang, Study on restraint stiffness of a four-angle assembled steel buckling-restrained brace, China Civil Engineering Journal. 45 (11) (2012) 79-87.

[24] Y.Q. Long, S.H. Bao, S. Yuan, Basic Course in Structural Mechanics, fourth ed, Chinese, Beijing, 2018.

[25] Y.J. Shi, Y.Q. Wang, M. Cheng, Design Method for Flexural Buckling of Webs in Aluminum Alloy Beams, J. Civ. Archit. Environ. Eng. 31(04) (2009) 1-5.